Research Paper

Ultrathin Cu-TCPP MOF nanosheets: a new theragnostic nanoplatform with magnetic resonance/near-infrared thermal imaging for synergistic phototherapy of cancers

Bo Li, Xiaoya Wang, Lei Chen, Yanling Zhou, Wentao Dang, Jiang Chang, Chengtie Wu✉

State Key Laboratory of High-Performance Ceramics and Superfine Microstructure, Shanghai Institute of Ceramics, Chinese Academy of Sciences, Shanghai 200050, China.

✉ Corresponding author: Chengtie Wu, Email: chengtiewu@mail.sic.ac.cn (C. Wu). Tel+86-21-52412249, Fax +86-21-52413903

Abstract

Nanostructures based on metal-organic frameworks (MOFs) have promising potential as theragnostic nanoplatforms for phototherapy of cancer cells. However, the MOFs alone are seldom reported to be used as photothermal agents mainly due to their poor near-infrared (NIR) light absorption.

Methods: Ultrathin copper-tetrakis (4-carboxyphenyl) porphyrin (Cu-TCPP) MOF nanosheets were prepared by a facile solvothermal route. The photothermal therapy (PTT), photodynamic therapy (PDT), and T_1-weighted magnetic resonance (MR) imaging capabilities and the high biocompatibility of these composite nanosheets were evaluated *in vitro* as well as *in vivo* in a mouse tumor model.

Results: The ultrathin Cu-TCPP MOF nanosheets exhibited 1) strong NIR absorption because of the d-d energy band transition of Cu^{2+} and the ultrathin characteristic translating into excellent photothermal performance, 2) ability to produce singlet oxygen because of the inherent characteristic of TCPP, and 3) capability for MR imaging because of the unpaired $3d$ electrons of copper.

Conclusion: Our study demonstrated that the Cu-TCPP MOF nanosheets are a promising phototherapy nanoplatform with the synergistic ability for PTT and PDT of cancer, guided by MR and infrared thermal imaging.

Key words: metal-organic frameworks, Cu-TCPP nanosheets, imaging, phototherapy

Introduction

As newly emerging porous materials, metal-organic frameworks (MOFs), constructed by the combination of metal ions or clusters with polytopic organic ligands, have drawn extensive attention as potential candidates for catalysts, sensors, gas separators, and biomedicines [1, 2]. Especially, MOFs show great potential in phototherapy of cancer cells due to their intrinsic biodegradability, high porosity, structural/chemical diversity, and highly enriched functionality [3-7]. Compared with traditional clinical cancer therapies, photothermal therapy (PTT) and photodynamic therapy (PDT) can be easily triggered by light as a minimally invasive approach [8]. MOFs can be used as photosensitizers (PS) in PDT to kill nearby cancer cells by generating toxic singlet oxygen (SO). Also, MOF-based materials as PTT agents can transfer light energy into heat under near-infrared (NIR) light irradiation, leading to hyperthermia in tumors.

For the construction of MOFs, special organic ligands, such as a commercially available PS used in PDT, tetrakis (4-carboxyphenyl) porphyrin (TCPP), can be employed. The resultant MOFs can be directly applied as effective PS for PDT [5, 9]. To achieve photothermal performance, MOF-based nanocomposites, which combine the advantages of MOFs and

traditional PTT agents, were developed [3, 4, 10]. However, these nanocomposites require complicated synthetic procedures. Polyaniline MOF hybrids and mesoporous carbon nanospheres containing porphyrin-like zinc centers can be used as MOF-based nanocomposites for PTT of cancers [3, 4]. The MOFs alone are seldom used as PTT agents due to their poor NIR light absorption properties. It has been shown that the two categories of phototherapies (*i.e.*, PDT and PTT) could work in a synergistic manner to kill cancer cells as the photothermal effect enhances the efficacy of PDT by relieving tumor hypoxia [11-13]. Therefore, a simplified method for the synthesis of MOF nanomaterials to function as NIR-triggered PDT and PTT agents is highly desirable.

It has been demonstrated that two-dimensional (2D) nanosheets show better photothermal performance than bulk materials due to their extreme thinness that allows them to respond rapidly to external light [14, 15]. Several kinds of 2D nanomaterials, such as graphene and graphene oxides [16, 17], metal oxides [18], and transition metal dichalcogenides (TMDs) [14, 15, 19], have been extensively investigated for PTT. Recently, 2D MOF nanosheets, as a new member of the 2D family, were successfully prepared [20]. In particular, the specific functionality of MOFs could be achieved by changing the categories of metal ions and ligands [21]. Previously, we have shown that Cu(II) in copper-based nanostructures exhibit NIR light absorption properties [22]. Thus, 2D Cu-TCPP MOF nanosheets may possess the ability for both SO generation and NIR absorption for phototherapy of cancers. Recently, there have been a few studies on 2D Cu-TCPP MOF nanosheets, but no information is available related to the PDT/PTT application. Therefore, exploring the bio-application of Cu-TCPP MOF nanosheets in cancer therapy would be of great significance.

In this study, ultrathin Cu-TCPP MOF nanosheets were prepared by a facile solvothermal method. In the Cu-TCPP MOF nanosheets, Cu^+ and Cu^{2+} coexist, leading to the strong NIR absorption due to the d-d energy band transition of Cu^{2+}. The 808 nm laser irradiation of Cu-TCPP MOF nanosheets resulted in effective heating due to their strong NIR absorption. The nanosheets also possess T_1-weighted magnetic resonance (MR) imaging capability because of the unpaired 3d electrons of copper. Furthermore, the Cu-TCPP MOF nanosheets can generate SO due to the inherent property (i.e., SO generation) of TCPP. Finally, we successfully demonstrated that the ultrathin Cu-TCPP MOF nanosheets could be used as an efficient "all-in-one" theragnostic agent for MR/IR thermal imaging and synergistic phototherapy of cancers. To the best of our knowledge, this is the first report on the bioapplication of imaging-guided phototherapy by using ultrathin Cu-TCPP MOF nanosheets.

Methods

Materials

All chemicals, unless specified otherwise, were purchased from Sinopharm Chemical Reagent Co., Ltd. (Shanghai, China) and used without further purification. Tetrakis (4-carboxyphenyl) porphyrin (TCPP) was obtained from TCI, Shanghai, China.

Synthesis of ultrathin Cu-TCPP MOF nanosheets

Twenty milligrams of TCPP and 0.5 g of polyvinylpyrrolidone (PVP) were dissolved in 16 mL N,N-dimethylformamide (DMF) in a vial under magnetic stirring. Subsequently, 4 mL of $Cu(NO_3)_2$ stock solution (25 mg/mL of $Cu(NO_3)_2$ in DMF) was added. After stirring for 2 min, the reaction mixture was kept in an 80 °C oven for 24 h. The product was collected by centrifugation and washed with ethanol and water.

Characterization

The morphology, size, and microstructure of Cu-TCPP MOF nanosheets were determined using a transmission electron microscope (TEM; JEM-2010F; Japan) and scanning electron microscope (SEM; S-4800; Japan). Energy-dispersive X-ray spectroscopy (EDS) of the sample was carried out using a Bruker Quantax 400 EDS system attached to a Hitachi S-4800 field emission scanning electron microscope. XRD measurements were performed on a D/max-2550 PC X-ray diffractometer (XRD; Rigaku, Japan). UV-vis absorbance spectra were measured at room temperature using a UV-visible-NIR spectrophoto-meter (Shimadzu UV-3600; Japan). XPS measure-ments were performed by X-ray photoelectron spectroscopy (XPS; ESCALab250; USA). Fluorescence intensity of singlet oxygen sensor green (SOSG) was examined at room temperature under a steady state/transient fluorescence spectrometer (QM/TM; USA). The concentration of copper ions released from Cu-TCPP in the solution was determined by inductively coupled plasma atomic emission spectroscopy (ICP-AES; Prodigy; USA). 808 nm semiconductor lasers were purchased from Shanghai Xilong Optoelectronics Technology Co. Ltd., China, whose power could be adjusted externally (0-2 W). The output power of the lasers was independently calibrated using a hand-held optical power meter (Newport model 1918-C, CA, USA). Confocal fluorescence imaging of cells was performed using a Leica SP5 laser scanning confocal microscope.

To measure the photothermal performance, 100 µL of Cu-TCPP MOF nanosheets of various concentrations were irradiated by an 808 nm semiconductor laser device at a power density of 1.0 W cm^{-2} (~316 mW for a spot size of ~0.316 cm^2) for 5 min. The temperature was monitored by a thermal imaging camera (FLIR A300, USA).

Singlet oxygen generation ability

To assess the generation of singlet oxygen, SOSG at a concentration of 5 µM was mixed with Cu-TCPP MOF nanosheets. Each solution was added to a 1 mL quartz cuvette, which was irradiated with a 660 nm laser (10 mW cm^{-2}) for the specified time. After irradiation, the nanosheets were removed by centrifugation. The SOSG fluorescence emission at 525 nm was measured following excitation at 504 nm.

For determination of ROS levels by fluorescence imaging, Saos-2 cells were cultured with or without Cu-TCPP nanosheets for 6 h in 4 different groups: control group, NIR group (660 nm, 10 mW cm^{-2}, 15 min), Cu-TCPP group (0.5 mg mL^{-1}), and Cu-TCPP+NIR group (0.5 mg mL^{-1}, 660 nm, 10 mW cm^{-2}, 15 min). Then, the fluorescent dye was added and co-incubated for 50 min. The NIR and Cu-TCPP+NIR groups were irradiated by 660 nm NIR laser light (10 mW cm^{-2}, 15 min). Subsequently, the medium was replaced with PBS, and ROS level was determined by fluorescence microscopy.

MR imaging

Cu-TCPP MOF nanosheets with various concentrations (0-5.18 mM) were scanned using an MR imaging scanner (MesoQMR23-060H-I) at room temperature. The longitudinal relaxivity r_1 was calculated as the reciprocal of T_1 ($r_1 = 1/T_1$) at various copper concentrations. For *in vivo* MR imaging, Saos-2 tumor-bearing nude mice were intratumorally injected with Cu-TCPP MOF nanosheets (100 µL, 5.18 mM) when the tumor size reached about 10 mm. Small animal MR images were collected and analyzed on an MR imaging scanner equipped with a special animal imaging coil. All animal experiments were performed in accordance with the guidelines of the Institutional Animal Care and Use Committee.

Cell viability

The *in vitro* cytotoxicity was evaluated using Cell Counting Kit-8 (CCK-8) (Dojindo Laboratories, Kumamoto, Japan). Saos-2 cells were seeded in a 96 well-plate at 1×10^4 cells per well and cultured at 37 °C in the presence of 5% CO_2. After incubation for 24 h, the Cu-TCPP MOF nanosheets dispersed in PBS were added to the wells at various concentrations and incubated for another 24 h. 10 µL of CCK-8 was added to each well of the plate. After incubation for 2 h, the optical density was measured at 450 nm using a microplate reader. All experiments were independently performed 4 times.

In vitro phototherapy

Saos-2 cells were seeded in a 96-well plate at a density of 1×10^4 cells per well and allowed to grow at 37 °C in the presence of 5% CO_2 for 24 h before treatment. The cell medium was removed, and the cells were washed with PBS buffer solution 3 times. The cells were divided into 6 groups: (1) PBS, (2) Cu-TCPP MOF nanosheets, (3) PBS + PTT + PDT, (4) Cu-TCPP MOF nanosheets + PDT, (5) Cu-TCPP MOF nanosheets + PTT, and (6) Cu-TCPP MOF nanosheets + PTT + PDT. Subsequently, 100 µL of PBS or various concentrations of the Cu-TCPP MOF nanosheets dispersed in PBS were then added to the wells. After incubation for another 12 h, the cells were washed with PBS 3 times. Next, the cells were irradiated by an 808 nm laser (1.0 W cm^{-2} for 10 min) and/or 660 nm laser (10 mW cm^{-2} for 30 min). Cell viability was measured by the CCK-8 assay. All tests were independently performed 6 times.

To visually compare the viability difference among 6 groups, Saos-2 cells were seeded into a 24-well plate at a density of 1×10^5 cells per well. After the cells were treated as described above, the cells were stained with calcein AM (transmits into the membranes of live cells) and propidium iodide (transmits into the membranes of dead cells) to distinguish live cells with green fluorescence and dead cells with red fluorescence. The procedure of Live/Dead assay was as follows: after indicated treatments, the cells were washed with fresh culture medium and then incubated with 500 µL mixture of propidium iodide and calcein AM for 30 min. The green fluorescence and/or red fluorescence emitted from the cells was observed using a confocal laser scanning microscope (Leica TCS SP8).

In vivo infrared thermal imaging

The mice bearing Saos-2 tumors were intratumorally injected with 100 µL of Cu-TCPP MOF nanosheets (1.0 mg/mL) or PBS. Thirty minutes after the injection, the mice with or without the Cu-TCPP MOF nanosheets injection were irradiated with the 808 nm laser at a power density of 1.0 W cm^{-2} (~0.316 W for a spot size of ~0.316 cm^2) for 5 min. During the laser irradiation, full-body infrared thermal images were captured using an infrared camera from a photothermal therapy monitoring system GX-A300 (Shanghai Guixin Corporation).

In vivo phototherapy

When the tumor reached about 10 mm, mice were randomly divided into 6 groups (5 mice per

group): (1) PBS, (2) Cu-TCPP MOF nanosheets, (3) PBS + PTT + PDT, (4) Cu-TCPP MOF nanosheets + PDT, (5) Cu-TCPP MOF nanosheets + PTT, and (6) Cu-TCPP MOF nanosheets + PTT + PDT. Mice bearing Saos-2 tumors were intratumorally injected with Cu-TCPP MOF nanosheets (1.0 mg/mL). Phototherapy treatments were then conducted with the 808 nm laser (1.0 W cm^{-2}, 10 min) for PTT and/or with the 660 nm laser (10 mW cm^{-2}, 30 min) for PDT. Twenty-four hours after different treatments, one mouse in each group was sacrificed, and the tumors were collected and prepared for hematoxylin and eosin (H&E) staining. The tumor sizes were measured using calipers every 2 days and calculated following the formula, volume = (tumor length) × (tumor width)^2/2. Relative tumor volumes were calculated as V/V_0 (V_0 was the tumor volume when the treatment was initiated).

Histological analysis

Healthy mice were intravenously injected with 100 µL of Cu-TCPP nanosheets dispersed in PBS at a dosage of 25 mg/kg. For controls, mice were intravenously injected with 100 µL of PBS solution. One month after the injection, major organs from both treatment and control groups were harvested, including the heart, lung, liver, spleen, and kidney. The histological examination of organs was performed by microscopy.

Results and discussion

Design and characterization of the Cu-TCPP MOF nanosheets

A facile solvothermal method was used to prepare ultrathin Cu-TCPP MOF nanosheets by heating Cu(NO$_3$)$_2$ and TCPP in N, N-dimethylformamide (DMF) at 80 °C for 24 h (**Figure 1A**). Polyvinylpyrrolidone (PVP) was used as a surfactant and surface ligand to control the shape of the required Cu-TCPP MOF nanostructures and improve their biocompatibility [20]. The Cu-TCPP MOF nanosheets prepared by this method were hydrophilic without any further modification and could remain stable when dispersed in water for at least 3 months and in PBS/RPMI-1640 culture medium for a week (**Figure S1A**). The nanosheets retained their strong NIR absorption at room temperature for a week, indicating good dispersion in water/PBS/RPMI-1640 culture medium (**Figure S1B-D**).
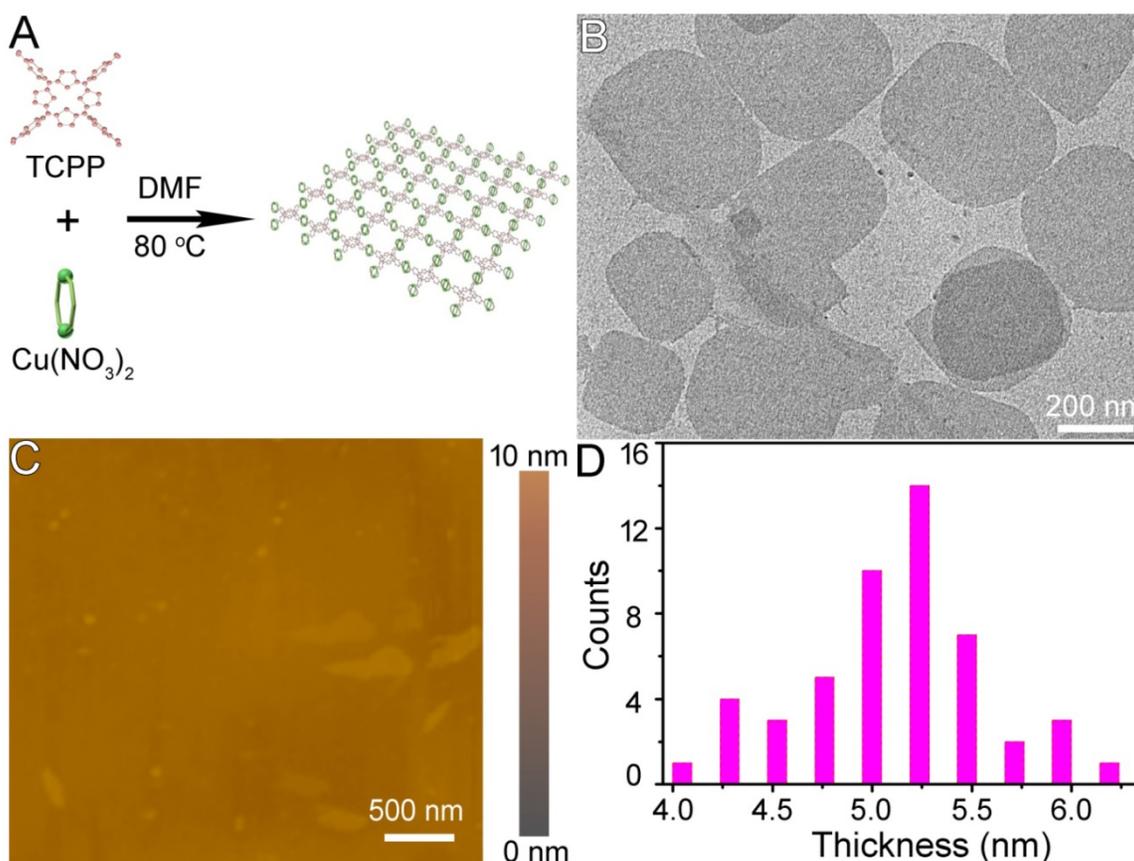

Figure 1. (A) Schematic illustration of the synthesis of Cu-TCPP MOFs. **(B)** TEM and **(C)** AFM images of Cu-TCPP MOF nanosheets. **(D)** Size histogram representing the thickness distribution of Cu-TCPP MOF nanosheets from AFM images.

The end products of the reaction were deposited at the bottom of the vessel with a clear yellow upper solution indicating that the reaction was complete. At this point, the yield of Cu-TCPP MOF nanosheets reached 85.36% ± 2.63% which was much higher than previously reported [20]. When measured by X-ray diffraction (XRD), a broad peak at ~18° was observed (**Figure S2A**), which is considered to be a typical peak of 2D nanosheets [20, 23, 24]. Scanning electron microscopy (SEM) demonstrated that the end products of the reaction were 2D nanosheets (**Figure S2B**). The Cu-TCPP MOF nanosheets were then characterized by transmission electron microscopy (TEM). Regardless of their size, the nanosheets laid flat on the TEM grid, indicating the thin nature of the nanosheets (**Figure 1B**). Atomic force microscopy (AFM) measurements of individual nanosheets confirmed the diameter with a very uniform thickness of 5.1 nm ± 0.3 nm. The average size of Cu-TCPP MOF nanosheets was around 330 nm as measured by dynamic light scattering (DLS) (**Figure S3**). The composition and chemical bonding state of the products were examined by X-ray photoelectron spectroscopy (XPS), showing that the nanosheets were mainly composed of Cu, C, O and N elements without any noticeable impurities (**Figure S4**). EDS analysis further confirmed that there were only Cu, C, O and N elements in the sample (**Figure S5**). These results confirmed the successful synthesis of the ultrathin Cu-TCPP MOF nanosheets.

Light absorption in the NIR region is a prerequisite for NIR-induced PTT agents. Materials with strong NIR absorption are considered to be good photothermal agents for PTT. Porphyrin-based sensitizers have been widely used as PS in PDT and approved by the U.S. Food and Drug Administration (FDA) [25]. However, they are seldom applied in PTT due to their poor NIR absorption. We examined the optical and photothermal properties of TCPP (**Figure S6**). TCPP dispersed in DMF showed zero absorption in the NIR region (from 800 nm to 1100 nm), and thus exhibited a very poor photothermal performance. In contrast, the Cu-TCPP MOF nanosheets showed a strong NIR absorption. **Figure 2A** displays the UV-vis-NIR absorbance spectrum of the aqueous dispersion containing 2D nanosheets. They exhibited a strong NIR absorption from 700 nm to 1100 nm, which was similar to the absorption of other 2D nanosheets [14, 15, 19]. When the concentration of Cu-TCPP MOF nanosheets was determined by ICP-AES, the extinction coefficient at 808 nm was 12.4 Lg^{-1} cm^{-1}, which was higher than that of graphene oxide and similar to that of gold nanorods [19]. Previously reported copper-based nanostructures were PTT active due to nonequivalent valency ions (*i.e.*, Cu^+ and Cu^{2+}), which led to ionized free carriers for achieving NIR absorption [22, 26]. We analyzed the valence state of Cu in Cu-TCPP. **Figure 2B** shows the Cu 2p spectrum for Cu-TCPP. The binding energy at 944.0 eV was assigned to the shake-up satellite peak of Cu^{2+}; a Cu $2p_{3/2}$ (934.8 eV) peak and a Cu $2p_{1/2}$ (954.7 eV) peak as well as two shakeup satellites in the Cu 2p spectrum confirmed the coexistence of two copper valence states, Cu^{2+} and Cu^+ [27]. The relative atomic percentages of Cu^{2+} and Cu^+ were determined by XPS to be 63% and 37%, respectively. We thus assigned the broad and strong absorbance intensity of the Cu-TCPP MOF nanosheets to rich copper vacancies from the unusual defect structures as well as the ultrathin character.

To investigate the photothermal properties, Cu-TCPP MOF nanosheets at concentrations of 0.125, 0.25, 0.50, and 1.0 mg/mL were exposed to the 808 nm NIR laser at a power density of 1.0 W cm^{-2}.
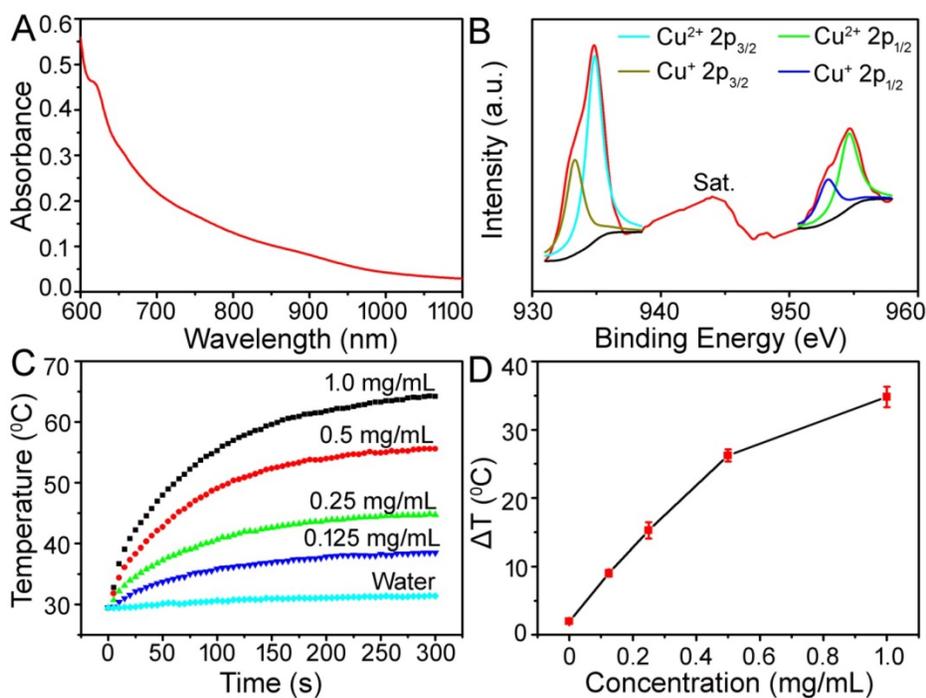

Figure 2. (A) UV-vis absorbance spectrum for the aqueous dispersion of the Cu-TCPP MOF nanosheets. **(B)** Cu 2p XPS spectrum for the Cu-TCPP MOF. **(C)** Temperature elevation of aqueous dispersions of Cu-TCPP MOF at different concentrations under irradiation with an 808 nm laser at a power density of 1.0 W cm^{-2}. **(D)** Plot of temperature change (ΔT) over a period of 300 s versus the concentration of MOF.

As shown in **Figure 2C-D**, the control experiment demonstrated that the temperature of pure water (without Cu-TCPP MOF nanosheets) only increased by less than 2.0 °C in 5 min. With the addition of the Cu-TCPP MOF nanosheets, the temperature of the aqueous dispersion increased by 9.0-34.5 °C after 5 min of irradiation, indicating that Cu-TCPP MOF nanosheets could rapidly and efficiently convert the 808 nm laser energy into heat energy due to strong photoabsorption at this wavelength.

For further assessment of the photothermal performance of the Cu-TCPP MOF nanosheets, we used a modified method similar to that used in our previous reports on $Cu_{7.2}S_4$ and $CuCo_2S_4$ nanocrystals (**Figure S7**) [26, 28]. The photothermal conversion efficiency, η_T, was calculated using the following equation:

$$\eta_T = \frac{hA(T_{max} - T_{amb}) - Q_0}{I(1 - 10^{-A_\lambda})} \quad (1)$$

In Equation 1, h is the heat transfer coefficient, A is the surface area of the container, T_{max} is the maximum system temperature, T_{amb} is the ambient surrounding temperature, ($T_{max} - T_{amb}$) is 26.2 °C, as shown in **Figure S7A**, I is the laser power (in units of W; 0.316 W), A_λ is the absorbance (0.6238) at the excitation wavelength of 808 nm, Q_0 is the heat input (in units of W) due to light absorption by the solvent. The lumped quantity hA was determined by measuring the rate of temperature drop after removing the light source. The value of hA was derived according to the following equation:

$$\tau_s = \frac{m_D C_D}{hA} \quad (2)$$

In Equation 2, τ_s (82.6 s) (**Figure S7B**) is the sample system time constant, m_D and C_D are the mass (0.1 g) and heat capacity (4.2 J g^{-1}) of deionized water, respectively, used as the solvent. Q_0 was measured independently and found to be 0.446 W. Thus, the 808

nm laser heat conversion efficiency of the Cu-TCPP MOF nanosheets was calculated to be 36.8%. We concluded that the Cu-TCPP MOF nanosheets could be used as excellent photothermal agents.

Singlet oxygen generation ability of Cu-TCPP MOF nanosheets

Porphyrinic MOF nanomaterials are a wide class of NIR-induced PDT photosensitizers [5, 6, 9]. To establish the intrinsic photodynamic properties of Cu-TCPP MOF nanosheets, we measured their SO generation ability by using the SOSG probe, an indicator of SO production whose green fluorescence can be recovered after reaction with SO. Under 660 nm light irradiation at a power density of 10 mW cm^{-2}, the fluorescence of SOSG incubated with Cu-TCPP MOF nanosheets increased gradually, suggesting the light-triggered production of SO. As shown in **Figure 3**, the Cu-TCPP MOF nanosheets exhibited both time-dependent and concentration-dependent SO generation ability, indicating their utility as an effective PDT agent. ROS generation by Cu-TCPP MOF nanosheets under NIR irradiation in cancer cells was evaluated by the fluorescent probe. The results in **Figure S8** show that the fluorescence signal in the experimental groups (Cu-TCPP + NIR) was higher than that observed in other groups, especially the control group.

Biocompatibility evaluation

The excellent photothermal performance and remarkable light-triggered production of SO by Cu-TCPP MOF nanosheets indicated their potential as promising phototherapy agents. Since Cu^{2+}ions are potentially toxic, we monitored Cu^{2+} release from Cu-TCPP MOF nanosheets in PBS before their potential bioapplication. There was a minimal release of $Cu^{2+}$from the nanosheets (**Figure S9**), indicating their low toxicity [26]. The cytotoxicity of Cu-TCPP MOF nanosheets was evaluated by CCK-8 assay in Saos-2 cells. As shown in **Figure 4A**, the nanosheets appeared to be minimally toxic as the cell viability was about 80% even at a high concentration of 3 mg/mL. The long-term toxicity of the Cu-TCPP MOF nanosheets was also investigated *in vivo.* The mice were given a single intravenous injection of nanosheets at a dosage of 25 mg/kg and sacrificed after one month. Various organs including the heart, lung, liver, spleen, and kidney were removed and stained with hematoxylin and eosin
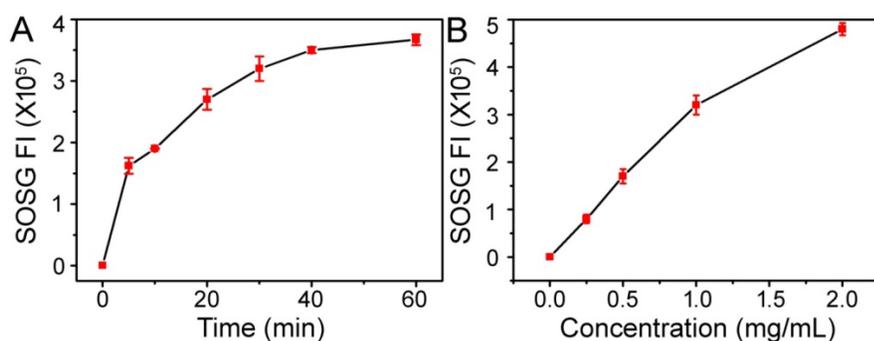

Figure 3. (A) Time-dependent generation of SOSG fluorescence under 660 nm light irradiation (10 mW cm^{-2}) with a 1.0 mg/mL concentration of Cu-TCPP MOF nanosheets. **(B)** Concentration-dependent generation of SOSG fluorescence under 660 nm light irradiation (10 mW cm^{-2}) for 30 min.
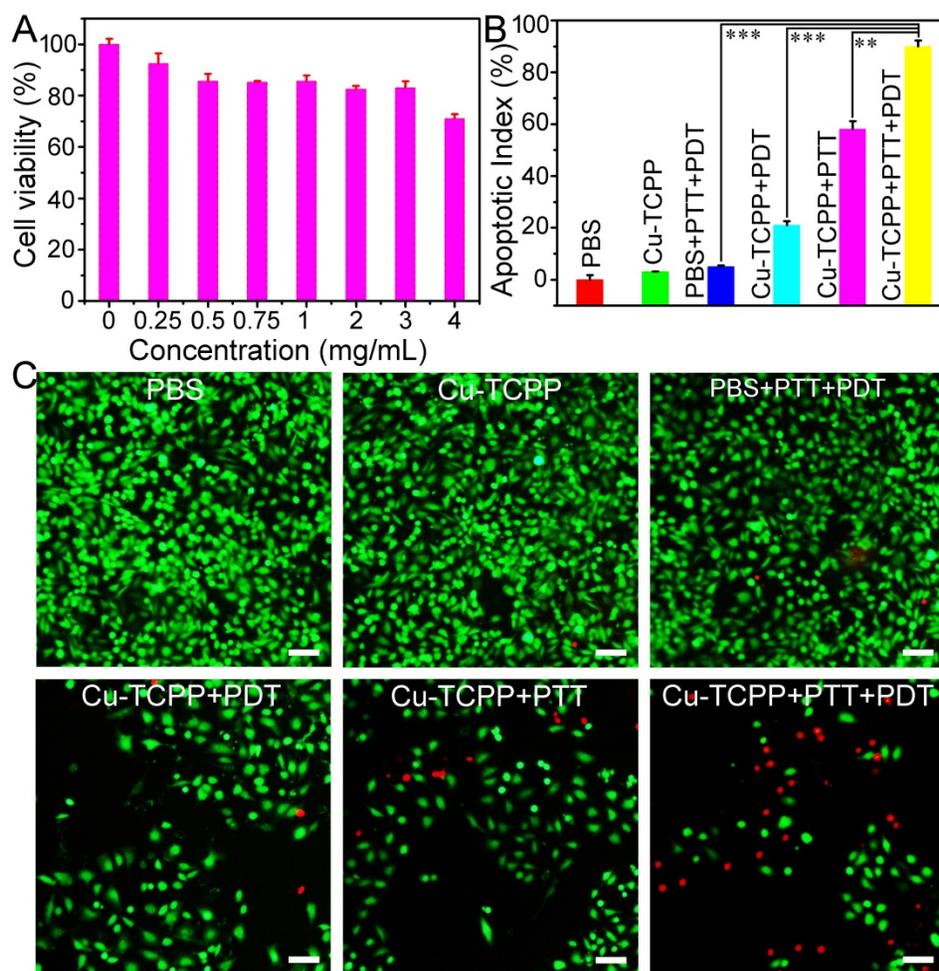
Figure 4. (A) Viability of Saos-2 cells incubated with different concentrations of Cu-TCPP MOF nanosheets for 24 h. **(B)** Cancer cell apoptosis after the indicated treatment with Cu-TCPP MOF nanosheets (1 mg/mL). P values: ***p < 0.001, **p < 0.01, or *p < 0.05. **(C)** Confocal images of calcein AM (green, live cells) and propidium iodide (red, dead cells) co-stained cells after incubation with Cu-TCPP MOF nanosheets for phototherapy. Scale bar: 20 µm.

(H&E). There was no obvious tissue damage or adverse effect associated with the administration of the Cu-TCPP MOF nanosheets, suggesting that the Cu-TCPP MOF nanosheets at the given dosage were not noticeably toxic.

In vitro phototherapy assay

The *in vitro* phototherapy performance of Cu-TCPP MOF nanosheets was examined in Saos-2 cells. As shown in **Figure 4B**, the CCK-8 assay demonstrated the high viability of cells treated with the laser or Cu-TCPP MOF nanosheets alone. However, the cell mortality rates for the Cu-TCPP + PDT group and the Cu-TCPP + PTT group were ~21% and ~58%, respectively. When the cells were treated with Cu-TCPP + PTT + PDT, the cell mortality increased significantly to ~90%. The half-maximal inhibitory concentration (IC50) of Cu-TCPP MOF nanosheets for combination phototherapy in Saos-2 cells was 0.43 mg mL^{-1}, while the IC50 for photothermal or photodynamic therapy alone was 0.82 mg mL^{-1} and 2.58 mg mL^{-1}, respectively. The

combination index (CI) was calculated to evaluate the synergistic effect of Cu-TCPP MOF nanosheets using photothermal and photodynamic therapy [29]. In this work, the CI value was 0.778, which demonstrated the synergistic effect of photothermal therapy and photodynamic therapy. Furthermore, to visualize the phototherapy efficiency, cells were co-stained with calcein-AM and propidium iodide (PI) following the indicated treatments (**Figure 4C**). The results were consistent with those of CCK-8 assay, further demonstrating the synergistic effect.

MR imaging

In addition to serving as phototherapy nanoplatforms, Cu-TCPP MOF nanosheets also have diagnostic applications. A variety of bioimaging technologies have been proposed for simultaneous diagnosis and therapy, thus enhancing therapeutic efficacy and minimizing side effects [12, 30]. In addition to their excellent phototherapy performance, the Cu-TCPP MOF nanosheets could be used as a magnetic resonance (MR) imaging contrast agent.

Metal ions with unpaired electrons, including Cu(II), Mn(II) and Gd(III), are candidates for T_1-weighted MR imaging contrast agents [31-33]. Because of the presence of Cu(II) in the Cu-TCPP MOF nanosheets (**Figure 2B**), we predicted that these nanosheets could be used as a T_1-weighted MR imaging contrast agent. To verify this notion, phantom images of aqueous dispersions of the Cu-TCPP MOF nanosheets and proton T_1 relaxation measurements at various Cu concentrations were performed using a 0.5T MR scanner. **Figure 5A** displays the T_1-weighted MR image of aqueous dispersions of the nanosheets at different concentrations. T_1-weighted MR signal intensity was enhanced with increasing concentration of nanosheets. The corresponding longitudinal relaxivity (r_1) of the nanosheets was calculated to be $r_1=0.52$ mM^{-1} s^{-1} from the slope of the reciprocal of T_1 ($r_1 = 1/T_1$) at various Cu concentrations (**Figure 5B**). To evaluate the T_1-weighted MR imaging capacity *in vivo*, Saos-2 tumor-bearing mice were imaged before and after intratumoral injection of Cu-TCPP MOF nanosheets dispersed in PBS. Following injection of the nanosheets, the tumor site exhibited sharp color contrast compared to the image before injection (**Figure 5C**), indicating that Cu-TCPP MOF nanosheets can be used as an effective contrast for T_1-weighted MR imaging of tumors.

In vivo infrared thermal imaging

We further investigated the *in vivo* NIR-induced thermal imaging of Cu-TCPP MOF nanosheets. An IR camera was used to capture full-body infrared thermal images and record the temperature change of the irradiated area. As expected, infrared thermal images with high contrast could be achieved (**Figure**

6A). For the mice injected with PBS (100 µL), the surface temperature of the irradiated area increased by less than 2 °C under irradiation with an 808 nm laser at a power density of 1.0 W cm^{-2} for 5 min. In the case of mice injected with Cu-TCPP MOF nanosheets solution (100 µL, 1.0 mg mL^{-1}), the tumor surface temperature increased from 31 °C to 45 °C under the same irradiation condition (**Figure 6B**). These results suggested that the Cu-TCPP MOF nanosheets maintained excellent photothermal effect *in vivo*.

In vivo phototherapy

Encouraged by the imaging data as well as positive PTT/PDT performance of Cu-TCPP MOF nanosheets under NIR irradiation, the combinational therapy effect using nude mice bearing Saos-2 tumors was verified. Tumors in mice were allowed to grow to a size of ~10 mm in diameter, following which mice were randomly divided into six groups with five mice per group: (1) PBS, (2) Cu-TCPP MOF nanosheets, (3) PBS + PTT + PDT, (4) Cu-TCPP MOF nanosheets + PDT, (5) Cu-TCPP MOF nanosheets + PTT, and (6) Cu-TCPP MOF nanosheets + PTT + PDT. PTT or PDT was conducted using either the 808 nm laser (1.0 W cm^{-2} for 10 min) or the 660 nm laser (10 mW cm^{-2} for 30 min). After the indicated treatments, the tumor sizes were measured using calipers every two days. **Figure 6C** shows the tumor volume change in representative mice from different groups as a function of time. The tumors in groups 1-3 showed fast growth rates, suggesting that treatment with only 808/660 nm laser irradiation or Cu-TCPP MOF nanosheets injection did not influence tumor development (**Figure 6C**). In marked contrast to the other groups in which PDT alone (group 4) or PTT alone (group 5) could slightly
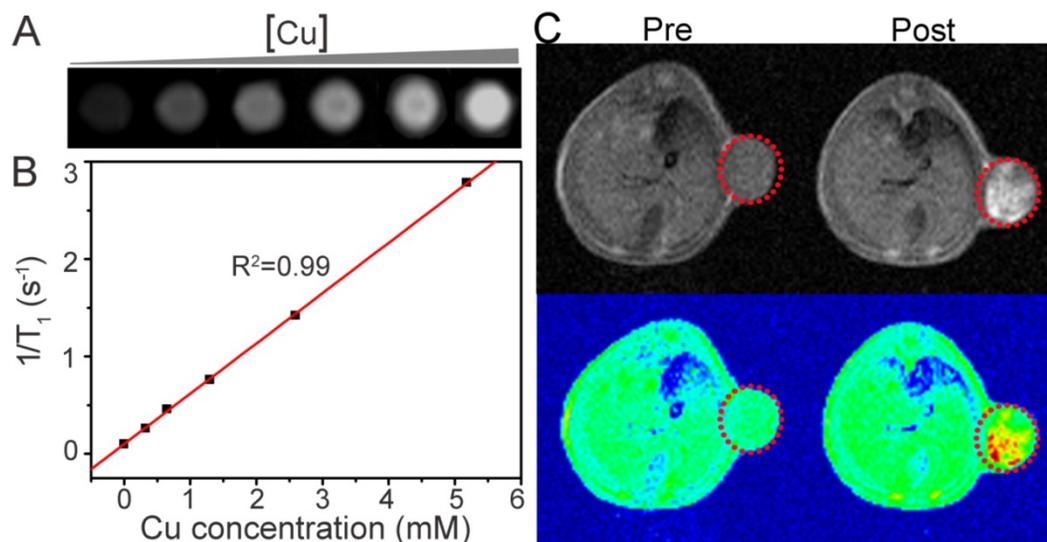

Figure 5. (A) *In vitro* T_1-weighted MR images of the Cu-TCPP MOF nanosheets with different aqueous dispersion concentrations. **(B)** Plots of the $1/T_1$ value of the Cu-TCPP MOF nanosheets as a function of concentration. **(C)** *In vivo* T_1-weighted MR views of a mouse before and after intratumoral injection of the Cu-TCPP MOF nanosheets solution. The position of the tumor is marked by red dotted circles.
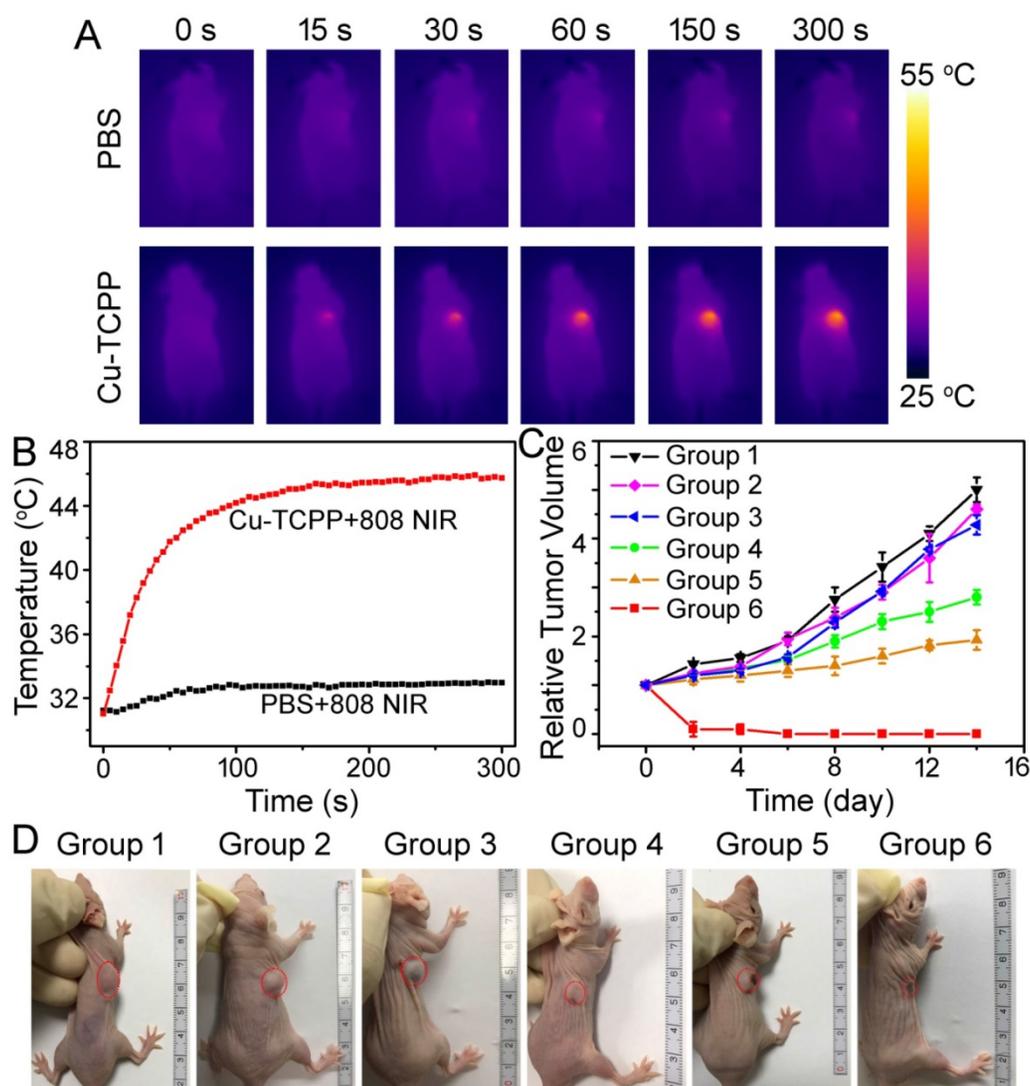
Figure 6. (A) Infrared thermal imaging of tumor-bearing mice after the intratumoral injection of PBS or nanosheets and exposure to 808 nm laser irradiation at a power density of 1.0 W cm^{-2}. **(B)** Temperature change curves of tumors in mice from (A) as a function of irradiation time. **(C)** Growth curves of tumors in mice from different treatment groups. Tumor volumes were normalized to their initial sizes. Error bars represent the standard deviations of 5 mice per group. **(D)** Representative photos of mice in different groups on day 14 after different treatments. The position of tumors is marked by the red dotted circles. Group 1: PBS; Group 2: Cu-TCPP; Group 3: PBS + PTT + PDT; Group 4: Cu-TCPP + PDT; Group 5: Cu-TCPP + PTT; Group 6: Cu-TCPP + PTT + PDT.

inhibit tumor growth, the tumors in group 6 completely regressed after the combined PTT + PDT treatment (**Figure 6C-6D**), indicating the synergistic effect of PTT and PDT. Histological examination of the tumor slices from each group was performed immediately after treatment. Cancer cells in control groups (groups 1-3) mainly retained their normal size and morphology and cancer cells in group 4 or group 5 were partially destroyed after PDT or PTT alone, while typical signs of cell damage were noticed in the tumors with the combined PTT + PDT therapy in group 6 (**Figure S11**). Compared with the three control groups, treatment in group 6 resulted in severe cellular damage, such as shrinkage of the malignant cells, nuclear condensation, fragmentation, and lysis. Thus, the combination of PTT + PDT therapy with Cu-TCPP MOF nanosheets was a highly

effective and feasible strategy for phototherapy of cancer cells.

Conclusions

In conclusion, hydrophilic Cu-TCPP MOF nanosheets with a mean thickness of ~5.1 nm were successfully prepared by a simple solvothermal route and employed as a novel imaging-guided phototherapy agent. The nanosheets had good dispersity and showed strong NIR absorption due to the d-d energy band transition of Cu^{2+} and their ultrathin character. The Cu-TCPP MOF nanosheets could generate SO due to the inherent property of TCPP, and demonstrated effective MR imaging derived from the unpaired electrons of Cu(II). Previously reported MOF-based phototherapy agents were mainly focused on MOF nanocomposites, in

which one part could be the PTT agent and the other the PDT agent. These systems needed complicated synthesis procedures with some of them requiring hydrophilic modification. In the present study, Cu-TCPP MOF nanosheets maintained the specific properties of each component. Significantly, the *in vitro* and *in vivo* toxicity studies indicated their good biocompatibility. Using NIR light irradiation and external magnetic field, the Cu-TCPP MOF nanosheets could be applied for MR/IR thermal imaging and synergistic phototherapy of cancers *in vivo*. Our study thus offers a novel type of ultrathin MOF nanosheets with multiple functionalities integrated within a single nanoscale system, which is useful for multimodal biomedical imaging-guided combinatorial cancer therapy.

Abbreviations

2D: two-dimensional; AFM: atomic force microscopy; CCK-8: Cell Counting Kit-8; CI: combination index; Cu-TCPP: copper-tetrakis (4-carboxyphenyl) porphyrin; DLS: dynamic light scattering; DMF: N, N-dimethylformamide; EDS: energy-dispersive X-ray spectroscopy; FDA: Food and Drug administration; H&E: hematoxylin and eosin; IC50: half-maximal inhibitory concentration; ICP-AES: inductively coupled plasma atomic emission spectroscopy; MOF: metal-organic framework; MR: magnetic resonance; NIR: near-infrared; PI: propidium iodide; PDT: photodynamic therapy; PS: photosensitizer; PTT: photothermal therapy; PVP: polyvinylpyrrolidone; SEM: scanning electron microscope; SO: singlet oxygen; SOSG: singlet oxygen sensor green; TCPP: tetrakis (4-carboxyphenyl) porphyrin; TEM: transmission electron microscopy; TMD: transition metal dichalcogenide; XRD: X-ray diffraction; XPS: X-ray photoelectron spectroscopy.

Supplementary Material

Supplementary figures S1-S11.
http://www.thno.org/v08p4086s1.pdf

Acknowledgements

Competing Interests

The authors have declared that no competing interest exists.

References

1. Peng Y, Li YS, Ban YJ, et al. Metal-organic framework nanosheets as building blocks for molecular sieving membranes. Science. 2014; 346: 1356-9.
2. Wang DD, Zhou JJ, Shi RH, et al. Biodegradable core-shell dual-metal-organic-frameworks nanotheranostic agent for multiple imaging guided combination cancer therapy. Theranostics. 2017; 7: 4605-17.
3. Wang S, Shang L, Li L, et al. Metal-organic-framework-derived mesoporous carbon nanospheres containing porphyrin-like metal centers for conformal phototherapy. Adv Mater. 2016; 28: 8379-87.
4. Wang WQ, Wang L, Li Y, et al. Nanoscale polymer metal-organic framework hybrids for effective photothermal therapy of colon cancers. Adv Mater. 2016; 28: 9320-5.
5. Liu J, Yang Y, Zhu W, et al. Nanoscale metal−organic frameworks for combined photodynamic & radiation therapy in cancer treatment. Biomaterials. 2016; 97: 1-9.
6. Park J, Jiang Q, Feng DW, et al. Size-controlled synthesis of porphyrinic metal-organic framework and functionalization for targeted photodynamic therapy. J Am Chem Soc. 2016; 138: 3518-25.
7. Lu KD, He CB, Lin WB. A chlorin-based nanoscale metal-organic framework for photodynamic therapy of colon cancers. J Am Chem Soc. 2015; 137: 7600-3.
8. Cheng L, Wang C, Feng LZ, et al. Functional nanomaterials for phototherapies of cancer. Chem Rev. 2014; 114: 10869-939.
9. Hu ZY, Pan YF, Wang JW, et al. Meso-tetra (carboxyphenyl) porphyrin (TCPP) nanoparticles were internalized by SW480 cells by a clathrin-mediated endocytosis pathway to induce high photocytotoxicity. Biomed Pharmacother. 2009; 63: 155-64.
10. Zhang H, Li YH, Chen Y, et al. Fluorescence and magnetic resonance dual-modality imaging-guided photothermal and photodynamic dual-therapy with magnetic porphyrin-metal organic framework nanocomposites. Sci Rep. 2017; 7: 441533.
11. Lin J, Wang SJ, Huang P, et al. Photosensitizer-loaded gold vesicles with strong plasmonic coupling effect for imaging-guided photothermal/photodynamic therapy. ACS Nano. 2013; 7: 5320-9.
12. Song G, Liang C, Gong H, et al. Core-shell MnSe@Bi₂Se₃ fabricated via a cation exchange method as novel nanotheranostics for multimodal imaging and synergistic thermoradiotherapy. Adv Mater. 2015; 27: 6110-7.
13. Gong H, Dong ZL, Liu YM, et al. Engineering of multifunctional nano-micelles for combined photothermal and photodynamic therapy under the guidance of multimodal imaging. Adv Funct Mater. 2014; 24: 6492-502.
14. Ren QL, Li B, Peng ZY, et al. SnS nanosheets for efficient photothermal therapy. New J Chem. 2016; 40: 4464-7.
15. Cheng L, Liu J, Gu X, et al. PEGylated WS₂ nanosheets as a multifunctional theranostic agent for in vivo dual-modal CT/photoacoustic imaging guided photothermal therapy. Adv Mater. 2014; 26: 1886-93.
16. Yang K, Hu LL, Ma XX, et al. Multimodal imaging guided photothermal therapy using functionalized graphene nanosheets anchored with magnetic nanoparticles. Adv Mater. 2012; 24: 1868-72.
17. Cheon YA, Bae JH, Chung BG. Reduced graphene oxide nanosheet for chemo-photothermal therapy. Langmuir. 2016; 32: 2731-6.
18. Song GS, Hao JL, Liang C, et al. Degradable molybdenum oxide nanosheets with rapid clearance and efficient tumor homing capabilities as a therapeutic nanoplatform. Angew Chem Int Edit. 2016; 55: 2122-6.
19. Chou SS, Kaehr B, Kim J, et al. Chemically exfoliated MoS₂ as near-infrared photothermal agents. Angew Chem Int Edit. 2013; 52: 4160-4.
20. Zhao MT, Wang YX, Ma QL, et al. Ultrathin 2D metal-organic framework nanosheets. Adv Mater. 2015; 27: 7372-8.
21. Furukawa H, Cordova KE, O'Keeffe M, , et al. The chemistry and applications of metal-organic frameworks. Science. 2013; 341: 974-9.
22. Li B, Ye K, Zhang Y, et al. Photothermal theragnosis synergistic therapy based on bimetal sulphide nanocrystals rather than nanocomposites. Adv Mater. 2015; 27: 1339-45.
23. Makiura R, Motoyama S, Umemura Y, et al. Surface nano-architecture of a metal-organic framework. Nat Mater. 2010; 9: 565-71.
24. Zheng J, Zhang H, Dong SH, et al. High yield exfoliation of two-dimensional chalcogenides using sodium naphthalenide. Nat Commun. 2014; 5:2995.
25. O'Connor AE, Gallagher WM, Byrne AT. Porphyrin and nonporphyrin photosensitizers in oncology: preclinical and clinical advances in photodynamic therapy. Photochem Photobiol. 2009; 85: 1053-74.
26. Tian Q, Jiang F, Zou R, Liu Q, Chen Z, Zhu M, et al. Hydrophilic Cu₉S₅ nanocrystals: a photothermal agent with a 25.7% heat conversion efficiency for photothermal ablation of cancer cells in vivo. ACS Nano. 2011; 5: 9761-71.

27. Liu HY, Xie JW, Liu P, et al. Effect of Cu$^+$/Cu^{2+} ratio on the catalytic behavior of anhydrous nieuwland catalyst during dimerization of acetylene. Catalysts. 2016; 6: 120.

28. Li B, Yuan FK, He GJ, et al. Ultrasmall CuCo$_2$S$_4$ nanocrystals: all-in-one theragnosis nanoplatform with magnetic resonance/near-infrared imaging for efficiently photothermal therapy of tumors. Adv Funct Mater. 2017; 27: 1606218.

29. Wang Y, Wang K, Zhao J, Liu X, Bu J, Yan X, et al. Multifunctional mesoporous silica-coated graphene nanosheet used for chemo-photothermal synergistic targeted therapy of glioma. J Am Chem Soc. 2013; 135: 4799-804.

30. Tian Q, Hu J, Zhu Y, et al. Sub-10 nm Fe$_3$O$_4$@Cu$_{2-x}$S core-shell nanoparticles for dual-modal imaging and photothermal therapy. J Am Chem Soc. 2013; 135: 8571-7.

31. Terreno E, Castelli DD, Viale A, et al. Challenges for molecular magnetic resonance imaging. Chem Rev. 2010; 110: 3019-42.

32. Viswanathan S, Kovacs Z, Green KN, et al. Alternatives to gadolinium-based metal chelates for magnetic resonance imaging. Chem Rev. 2010; 110: 2960-3018.

33. Zhou M, Tian M, Li C. Copper-based nanomaterials for cancer imaging and therapy. Bioconjug Chem. 2016; 27: 1188-99.